Course:

ASEN 6367

Advanced Finite Element Methods

Project title:

Development and Test of an Improved 4-node Axisymmetric (ring) Element for Nearly Incompressible Materials

Prepared by:

Reza Behrou

Farhad Shahabi

May, 2013

Develop and Test of an Improved 4-node Axisymmetric (ring) Element for Nearly Incompressible Materials

Abstract

In this project, the hybrid element formulation is used to improve the performance of the 4-node quadrilateral element for nearly incompressible materials. Based on the numerical results of the class notes [1] the conventional 4-node element is not able to capture the displacement field for the nearly incompressible materials. The hybrid element formulation used in this project is based on the two master fields, the stress and the displacement fields at the boundaries. The performance of the developed element is evaluated by considering three benchmark problems.

Introduction

There are several motivations for constructing mixed functionals. In essence a multi-field functional is called mixed when there are multiple master fields involved. The original motivation of mixed functional is the famous Hellinger – Reissner (HR) functional of linear elasticity. In this functional both displacement and stress are independently varied. The main reason of using multi-field functional is the accuracy of the solution for the master fields. One of the most successful multi-field functional is based upon the concept of hybridization of the involved master fields. In this approach, the stress within the continuum and the boundary displacements are considered as master fields.

Finite elements based on hybrid functionals, called hybrid elements, were constructed in the early 1960s. The original elements were quite limited in their ability to treat nonlinear and dynamic problems, as well as treatment of complicated geometries. However, such limitations are gradually disappearing as the fundamental concepts are better understood. Presently hybrid principles represent an important area of research in the construction of high performance finite elements, especially for plates, shells, and near incompressible axisymmetric problems [1].

The hybridization principle is splitting the domain into a number of subdomains by considering the internal interfaces traction. The approximate solution to such a problem can be accomplished by using of the principle of total complementary potential energy. Recognizing the application of hybrid functional, the hybrid-stress-displacement formulation based on which an efficient axisymmetric solid of revolution element has been described below.

Hybrid Stress – Displacement formulation

In this project the hybrid finite element formulation is based on the division of the continuum domain in the sub-domain V^n. It is to be noted that instead of considering equilibrated stresses over the entire volume, the equilibrium conditions of the surface tractions T_i along the inter-element boundaries and along the prescribed stress boundaries need to be satisfied at once. The variational form of the hybrid functional which is based on the complementary total potential energy and the prescribed boundary traction can be defined as:

$$\Pi_{Hybrid} = \sum_n \left(\int_{v_n} \frac{1}{2} C_{ijkl} \sigma_{ij} \sigma_{kl} dv - \int_S T_i u_i dS + \int_{S_T} \bar{T}_i u_i dS \right) \tag{1}$$

Where C_{ijkl} is the elastic compliance tensor, σ_{ij} is the Cauchy stress tensor, u_i Is the boundary displacement, S is pa portionof the surface where T is prescribed, S_T is the inter-element boundary where $\bar{T}_i$ is prescribed. The component of the element boundary tractions T_i is related to the stress components by

$$\{T\} = [\sigma]\{n\} \tag{2}$$

In which n_j is the normal vector of the surface boundary. Thus the original complementary energy involves only the stress field as the variables while in the definition of the hybrid functional the inter-element boundary displacement u_i is the additional variables in the hybrid functional. The hybrid functional entails two master field, one known as the boundary displacement field and the other one is the element stress field. In the finite element formulation the assumed function for the approximation of the stress field throughout the element σ is defined by the coefficient matrix and the stress parameters β. It is to be noted that first of all the stress function need to satisfy the equilibrium equations and the biharmonic stress function. Upon fulfilling these two constraints, the number of stress parameters should be defined in a way that avoid the rank deficiency problem. The number of the stress parameters needs to be more than the total degree of freedom of the element minus the rigid body modes.

$$\{\sigma\} = [\boldsymbol{P}]\{\beta\} + [\boldsymbol{P_F}]\{\beta_F\} \tag{3}$$

In order to simplify the formulation it is assumed that the body force is zero. In the absence of body force the above equation can be expressed in this way

$$\{\sigma\} = [\boldsymbol{P}]\{\beta\} \tag{4}$$

The coefficient matrix P is a function of the coordinates systems, whereas β's are unknown parameters and upon obtaining the these unknowns the stress function over the element is fully defined.

The appropriate displacements along the inter-element boundaries are then interpolated in terms of the generalized nodal displacements **u** such that

$$\{U\} = [\boldsymbol{L}]\{u_i^e\} \tag{5}$$

It is to be noted that the definition of displacement over the boundary is different from the displacement over the whole element. Thus, the matrix L is not the same as those shape functions in the conventional finite element analysis .

By using equations (2) and (3) the boundary traction can be expressed in the following way

$$\{T\} = [\boldsymbol{R}]\{\beta\} + [\boldsymbol{R_F}]\{\beta_F\} \tag{6}$$

In the absence of body force the traction can be expressed such that

$$\{T\} = [\boldsymbol{R}]\{\beta\} \tag{7}$$

Upon substituting Eqs. 3, 5 and 6 into Eq. 1the Hybrid functional in its complete format by considering the body force is such that

$$\begin{aligned}\Pi_{Hybrid} = &\sum_n \left(\int_{v_n} \frac{1}{2}\left[\{\beta\}^T [H]\{\beta\} + \{\beta_F\}^T [H_{FF}]\{\beta_F\} + \{\beta\}^T [H_F]\{\beta_F\} \right] dv \right) \\ &- \sum_n \left(\int_S \left[\{\beta\}^T [R]^T L + \{\beta_F\}^T [R_F]^T L \right] \{u_i^e\} dS + \int_{S_T} \bar{T}_i L \{u_i^e\} dS \right)\end{aligned} \tag{8}$$

In which

$$H = \int_{v_n} [P]^T [C][P] dV \tag{9}$$

$$H_F = \int_{v_n} [P]^T [C][P_F] dV \tag{10}$$

$$H_{FF} = \int_{v_n} [P_F]^T [C][P_F] dV \tag{11}$$

Upon the assumption of zero body force terms, the hybrid functional Eq. 8 reduces as follows.

$$\beta_F = P_F = R_F = 0 \tag{12}$$

It is to be noted that by taking the body force into account we need to come up with the complicated stress function that need to fulfill the equilibrium equations and the biharmonic stress function which are the inhomogeneous partial differential equations. Thus, regardless of the body force the hybrid functional is such that

$$\Pi_{Hybrid} = \sum_n \left(\int_{v_n} \frac{1}{2} \{\beta\}^T [H] \{\beta\} dv \right) - \sum_n \left(\int_S \left(\{\beta\}^T [R]^T L \right) \{u_i^e\} dS + \int_{S_T} \bar{T}_i L \{u_i^e\} dS \right) \tag{13}$$

By manipulating the hybrid functional more we have

$$\int_S \left(\{\beta\}^T [R]^T L \right) \{u_i^e\} dS = \int_S T_i u_i dS \Rightarrow \int_S \sigma_{ij} u_i n_j dS \tag{14}$$

By using divergence theorem Eq. 14 turns out as

$$\int_{v_n} \sigma_{ij,j} u_i dv + \int_{v_n} \sigma_{ij} u_{i,j} dv = \int_{v_n} \sigma_{ij} \varepsilon_{ij} dv = \int_{v_n} [\sigma]^T [\varepsilon] dv \tag{15}$$

It is to be noted that the Eq. 15 is obtained based on the assumption of zero body force. The hybrid formulation can be rewritten as follows

$$\Pi_{Hybrid} = \sum_n \left(\int_{v_n} \frac{1}{2} \{\beta\}^T [H] \{\beta\} dv \right) - \sum_n \left(\int_{v_n} \left(\{\beta\}^T [P]^T [B] \right) \{u_i^e\} dv + \int_{S_T} \bar{T}_i L \{u_i^e\} dS \right) \tag{16}$$

It is worth to mention that in Eq. 16 the definition of strain is based on the B matrix likewise the conventional finite element analysis.

$$G = \int_{v_n} [P]^T [B] dv \tag{17}$$

By taking the variation of above hybrid formulation with respect to β we can come up with an expression that connect the stress parameters to the nodal displacements.

$$[H][\beta]-[G]\{u_i^e\}=0\Rightarrow[\beta]=[H]^{-1}[G]\{u_i^e\} \tag{18}$$

Upon plugging Eq. 18 into Eq. 16 we can come up with the Hybrid functional based on the nodal displacements as the only unknowns. We have

$$\Pi_{Hybrid}=-\sum_n\left(\int_{v_n}\frac{1}{2}\left(\{u_i^e\}^T[G]^T[H]^{-T}[G]\{u_i^e\}\right)dv\right)+\int_{S_T}\bar{T}_i L\{u_i^e\}dS \tag{19}$$

Taking the variation of the above function with respect to u_i^e the element stiffness matrix can be written as

$$K=[G]^T[H]^{-T}[G] \tag{20}$$

It is worth noticing that the above formulation is generic. Thus, for our purposes we need to employ the above formulation to construct the 4-node quadrilateral element appropriate for the axisymmetric analysis.

Axi-symmetric quadrilateral element

In order to formulate the axisymmetric element we need to be defined the displacement, stress and constitutive equations for the axisymmetric analysis.

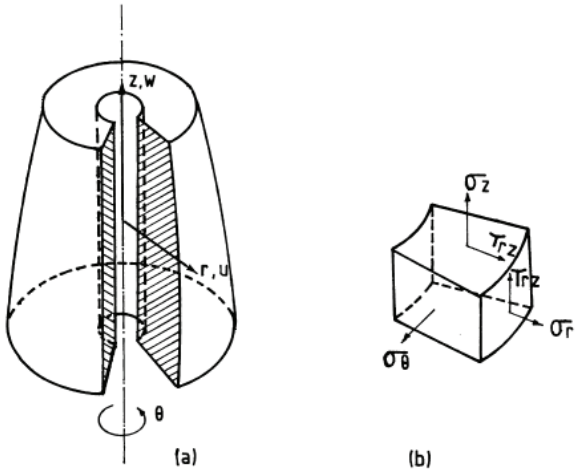

Figure 1. Axi-symmetric body: (a) body of revolution; and (b) four non-zero stress components on an infinitestimal volume of the axisymmetric continua [2].

The axisymmetric element has two displacement degree of freedom per node, one in radial and the other in the axial directions, So it can be written as

$$\boldsymbol{u} = \{u, w\}^T \tag{21}$$

Where u and w are the displacements in the r and z directions, respectively. The non-zero strain are

$$\boldsymbol{\varepsilon} = \{\varepsilon_z, \varepsilon_\theta, \varepsilon_r, \gamma_{rz}\}^T \tag{22}$$

Where based on the kinematics of the small strain problem the relation of the strains and displacement for the axisymmetric solid is such that

$$\begin{aligned} &\varepsilon_r = \frac{\partial u}{\partial r}, \quad \varepsilon_\theta = \frac{u}{r}, \quad \text{and } \varepsilon_z = \frac{\partial w}{\partial z} \\ &\gamma_{rz} = \frac{\partial u}{\partial z} + \frac{\partial w}{\partial r} \end{aligned} \tag{23}$$

The strain – stress constitutive equation based on the compliance matrix can be expressed as

$$\boldsymbol{\varepsilon} = \boldsymbol{C}\boldsymbol{\sigma} \tag{24}$$

Where $\sigma = \{\sigma_z, \sigma_\theta, \sigma_r, \tau_{rz}\}^T$ and $\varepsilon = \{\varepsilon_z, \varepsilon_\theta, \varepsilon_r, \gamma_{rz}\}^T$. For the linear elastic materials, the elastic compliance matrix is as follows

$$C = \frac{1}{E}\begin{bmatrix} 1 & -\nu & -\nu & 0 \\ -\nu & 1 & -\nu & 0 \\ -\nu & -\nu & 1 & 0 \\ 0 & 0 & 0 & 2(1+\nu) \end{bmatrix} \tag{25}$$

The approximation of the displacement field based on the four-node quadrilateral element's shape functions can be expressed as

$$u = \sum_{i=1}^{4} N_i(\xi, \eta) u_i \ , \quad w = \sum_{i=1}^{4} N_i(\xi, \eta) w_i \tag{26}$$

Where for node i, u_i and w_i are nodal displacements and $N_i(\xi, \eta)$ represents for the shape functions which are defined for the 4-node quadrilaterals as follows

$$N_i = (1 + \xi\xi_i)(1 + \eta\eta_i) \tag{27}$$

Where (ξ, η) are the local coordinates and (ξ_i, η_i) are the nodal coordinates in the parent domain. Thus, the B matrix for the axisymmetric 4-node quadrilateral element can be expressed as

$$\begin{bmatrix}\varepsilon_r\\ \varepsilon_z\\ \varepsilon_\theta\\ \gamma_{rz}\end{bmatrix}=\begin{bmatrix}\frac{\partial N_1^e}{\partial r} & 0 & \frac{\partial N_2^e}{\partial r} & 0 & \frac{\partial N_3^e}{\partial r} & 0 & \frac{\partial N_4^e}{\partial r} & 0\\ 0 & \frac{\partial N_1^e}{\partial z} & 0 & \frac{\partial N_2^e}{\partial z} & 0 & \frac{\partial N_3^e}{\partial z} & 0 & \frac{\partial N_4^e}{\partial z}\\ \frac{N_1^e}{r} & 0 & \frac{N_2^e}{r} & 0 & \frac{N_3^e}{r} & 0 & \frac{N_4^e}{r} & 0\\ \frac{\partial N_1^e}{\partial z} & \frac{\partial N_1^e}{\partial r} & \frac{\partial N_2^e}{\partial z} & \frac{\partial N_2^e}{\partial r} & \frac{\partial N_3^e}{\partial z} & \frac{\partial N_3^e}{\partial r} & \frac{\partial N_4^e}{\partial z} & \frac{\partial N_4^e}{\partial r}\end{bmatrix}\left\{u_i^e\right\}=\left[B\right]\left\{u_i^e\right\} \tag{28}$$

The appropriate stress functions for the axisymmetric element need to satisfy the equilibrium and biharmonic stress functions [2,3]. These functions for the axisymmetirc case can be expressed as

$$\frac{\partial\sigma_r}{\partial r}+\frac{\partial\tau_{rz}}{\partial z}+\frac{\sigma_r-\sigma_\theta}{r}=0 \tag{29}$$

$$\frac{\partial\sigma_z}{\partial z}+\frac{\partial\tau_{rz}}{\partial r}+\frac{\tau_{rz}}{r}=0 \tag{30}$$

$$\nabla^2\left(\sigma_r+\sigma_\theta+\sigma_z\right)=\left(\frac{\partial^2}{\partial r^2}+\frac{1}{r}\frac{\partial}{\partial r}+\frac{\partial^2}{\partial z^2}\right)\left(\sigma_r+\sigma_\theta+\sigma_z\right)=0 \tag{31}$$

There are several stress functions that you can propose for various analysis, one the stress functions that is able to capture the exact solution for the under pressure thick wall cylinder is as follows [2],

$$\begin{aligned}\sigma_z&=\beta_6+\beta_7 z-3\beta_3 r-\beta_4\frac{1}{r}-\beta_5\frac{z}{r}\\ \sigma_\theta&=\beta_1+\beta_2 z+2\beta_3 r\\ \sigma_r&=\beta_1+\beta_2 z+\beta_3 r+\beta_4\frac{1}{r}+\beta_5\frac{z}{r}\\ \tau_{rz}&=\beta_5-\frac{1}{2}\beta_7 r\end{aligned} \tag{32}$$

It is to be noted that it has seven stress parameters that need to be defined during the finite element solution to fully define the stress of the element. The function can be rewritten in terms of the coefficient matrix and stress parameters as follows.

$$[\sigma]=[P]\{\beta\}=\begin{bmatrix} 1 & z & r & 1/r & z/r & 0 & 0 \\ 0 & 0 & -3r & -1/r & -z/r & 1 & z \\ 1 & z & 2r & 0 & 0 & 0 & 0 \\ 0 & 0 & 0 & 0 & 1 & 0 & -1/2r \end{bmatrix} \begin{Bmatrix} \beta_1 \\ \beta_2 \\ \beta_3 \\ \beta_4 \\ \beta_5 \\ \beta_6 \\ \beta_7 \end{Bmatrix} \tag{33}$$

The stiffness matrix for the axisymmetric 4-node quadrilateral elements can be obtained by

$$K = [G]^T [H]^{-T} [G] \tag{34}$$

In which H and G matrices can be expressed as

$$H = 2\pi \int_{-1}^{1}\int_{-1}^{1} P^T C P \, r \det|J| \, d\xi \, d\eta \tag{35}$$

$$G = 2\pi \int_{-1}^{1}\int_{-1}^{1} P^T B \, r \det|J| \, d\xi \, d\eta \tag{36}$$

It is to be noted that these two matrices are dependent on the P matrix defined based on the selected stress function. Thus, the stress approximation functions play the crucial role in the hybrid finite element analysis. Since the selection of inappropriate stress approximation may deteriorate the performance of the hybrid elements.

Results and Discussion

In this section the developed hybrid finite element method is used to solve three benchmark problems for the nearly incompressible materials. It is to be noted that the stress function that is proposed in the formulation section is used for the simulation of all of these problems. The benchmarks are chosen from the Timoshenko and Krieger (1959) book in which the analytical solution is provided for these problems. The comparison of numerical results with analytical solution is the unique opportunity to test the performance of the hybrid finite element method. Three considered benchmark problems are under pressure thick wall cylinder, simply supported thin circular plate under point load and cantilevered thin circular plate under point load.

Benchmark No.1: Thick wall cylinder with internal pressure

The under pressure thick wall cylinder is the first model that is going to be discretized by the axisymmetric 4-node quadrilateral hybrid elements. Fig. 2 depicts the schematic of the mesh configuration and boundary conditions for the model. In addition, the geometrical and the material properties are expressed in the table. 1.

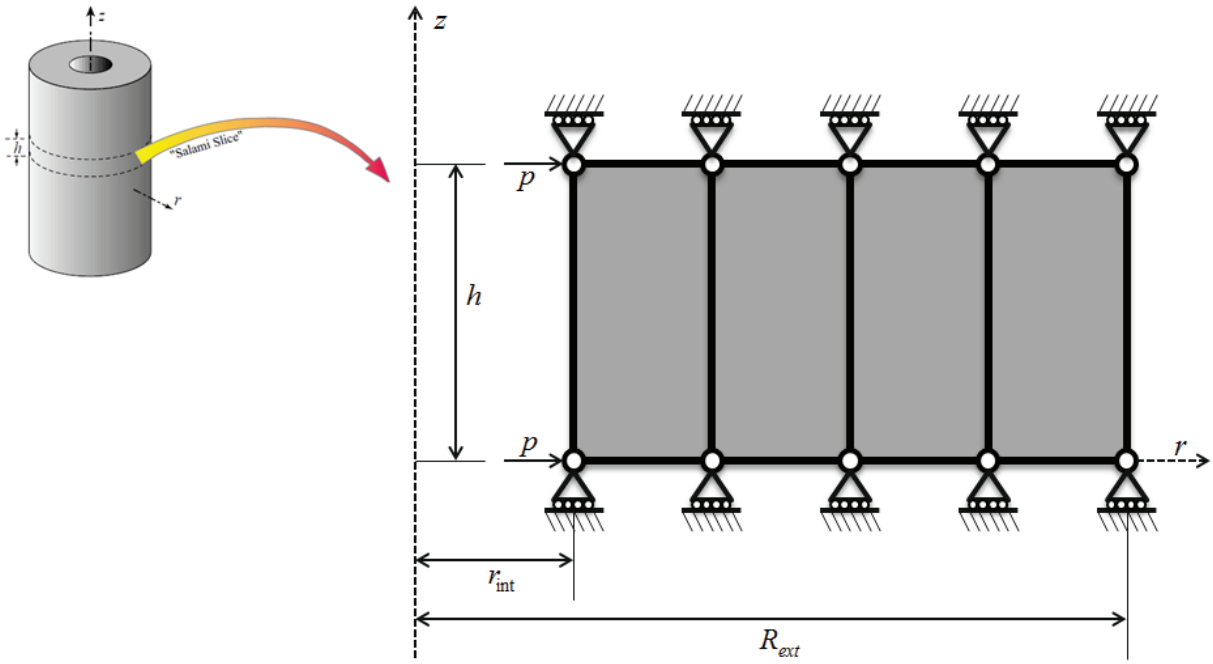

Figure 2. Thick wall cylinder under internal pressure

Table 1. The geometrical and material properties

Input Parameters	r_{int} (m)	R_{ext} (m)	h (m)	E (N/m^2)	v	p
Values	4.0	10.0	0.5	1.0e+05	0.4999999	10

Timoshenko [4] proposed the analytical solution for the under pressure thick wall as follows

$$
\begin{aligned}
u_z &= 0 \\
u_r &= p\,\frac{r_{int}^2\,(1+\nu)}{\left(R_{ext}^2 - r_{int}^2\right)}\left((1-2\nu)r - \frac{R_{ext}^2}{r}\right) \\
\sigma_r &= p\,\frac{r_{int}^2\left(\frac{R_{ext}^2}{r^2} - 1\right)}{\left(R_{ext}^2 - r_{int}^2\right)} \\
\sigma_\theta &= p\,\frac{r_{int}^2\left(\frac{R_{ext}^2}{r^2} + 1\right)}{\left(R_{ext}^2 - r_{int}^2\right)}
\end{aligned}
\tag{37}
$$

In which u_z is the axial displacement, which is zero, u_r represents for the radial displacement, σ_r is the radial stress and σ_θ is the definition of the hoop stress. Fig . 3 depicts the profile of the axial displacement versus the radius of the cylinder. The obtained numerical results are in good agreement with those obtained from the analytical procedure. Fig. 4 represents the contour plot of the axial stress versus the radius of the cylinder. From this figure it can be easily observed the variation of the compressive stress throughout the thickness. Fig. 5 illustrates the accuracy of the numerical results obtained from the hybrid finite element method in comparison with the analytical solution. The main advantage of the hybrid finite element method in comparison with the conventional finite element analysis is the accuracy of calculated stress field since it is a master field in the hybrid method. Fig. 6 is devoted to the contour plot of the hoop stress. The profile of hoop stress with respect to the thickness of the cylinder can be observed. Fig. 7 illustrates the accuracy of the hoop stress obtained from the finite element calculation in comparison with the analytical solution. It is to be noted that the stress values are calculated at the integration point and compared with the analytical solution at the integration point's locations.

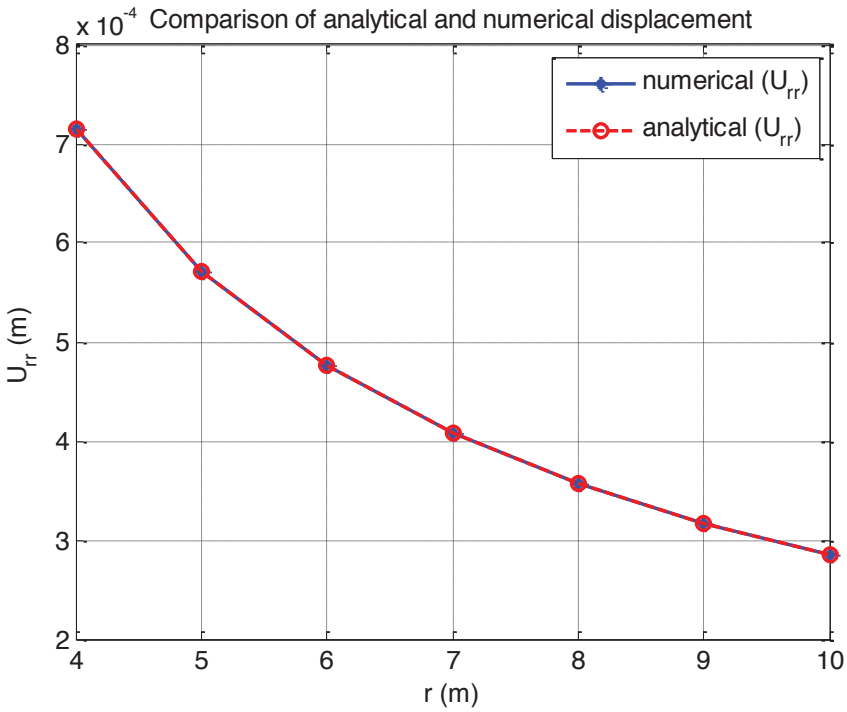

Figure 3. Comparison of analytical and numerical displacement - U_{rr}

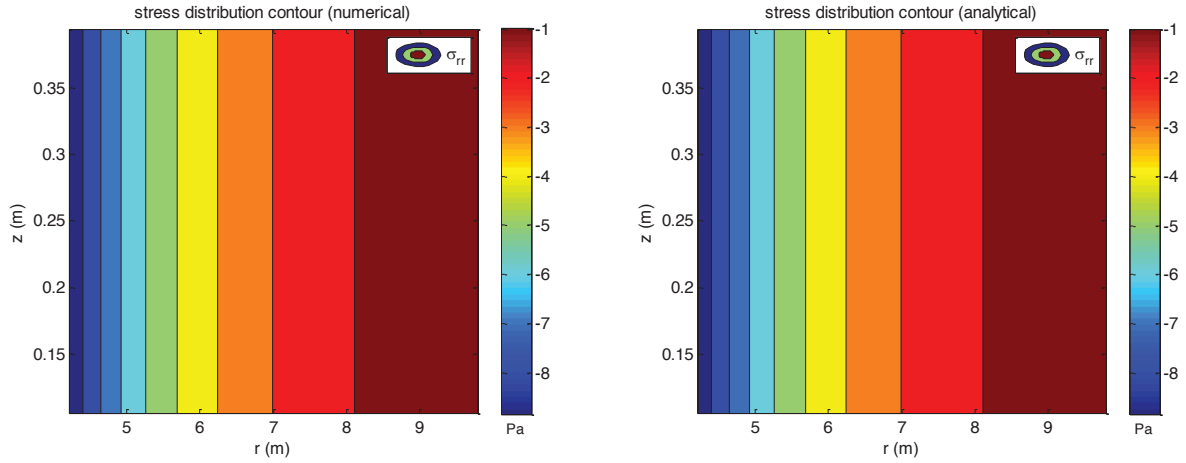

Figure 4. Radial stress distribution contour (σ_{rr}) – numerical & analytical results

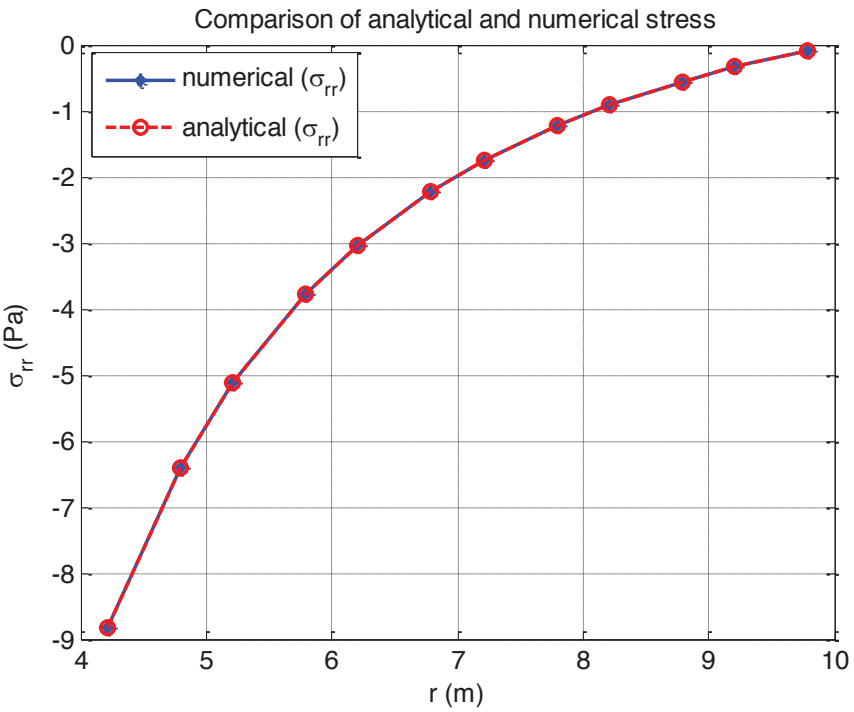

Figure 5. Comparison of analytical and numerical stress (σ_{rr})

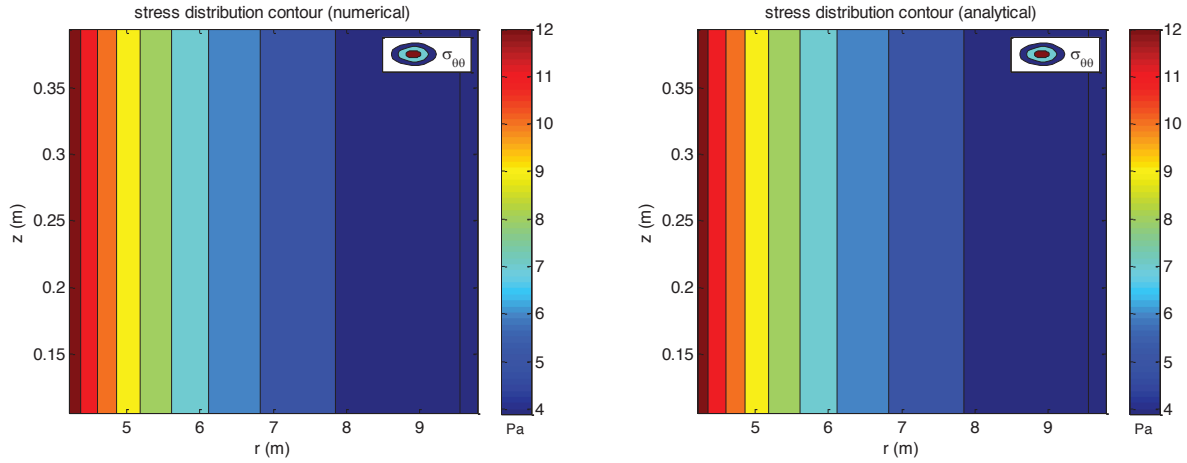

Figure 6. Circumferential stress distribution contour ($\sigma_{\theta\theta}$) – numerical & analytical results

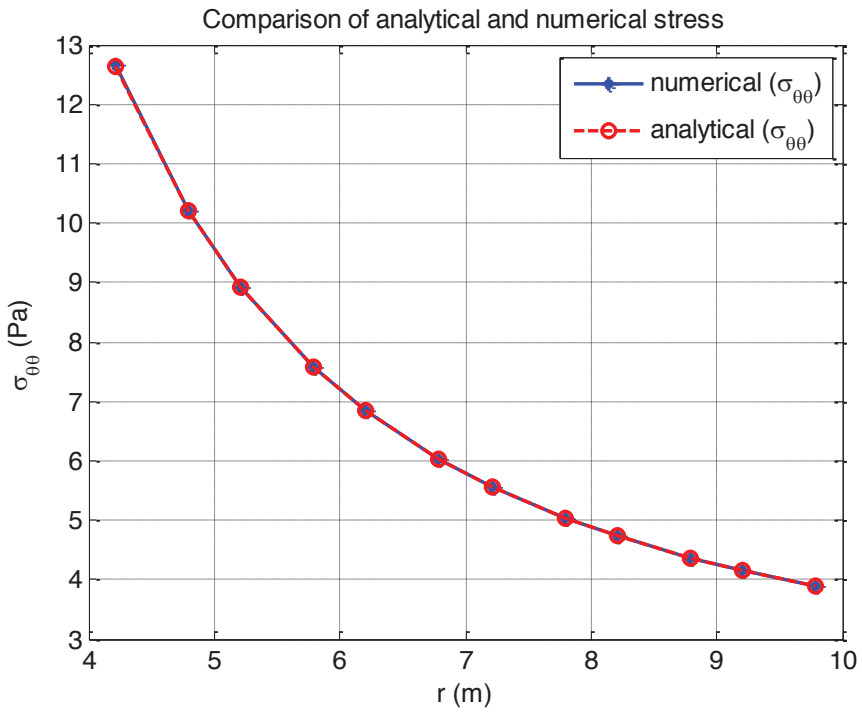

Figure 7. Comparison of analytical and numerical stress ($\sigma_{\theta\theta}$)

In the next section the thin circular plate with the simply supported boundary conditions is considered. It is to be noted that the same stress function as the one used for the analysis of the thick wall cylinder is employed.

Benchmark No.2: Simply supported circular plate with point load

In this section a thin simply supported circular plate is discretized by the 4-node quadrilateral element in the framework of the hybrid finite element method. Fig. 8 depicts the schematic of the model and the mesh configuration used for the simulation. Table 2. Presents the material and geometrical properties of the considered model. The analytical solution for this problem is available in the Timoshenko [4].

Table 2. The geometrical and material properties for the simply supported circular plate

Input Parameters	***r (m)***	***h (m)***	***E (N/m^2)***	***v***	***p***
Values	4.0	0.5	1.0e+05	0.4999999	10

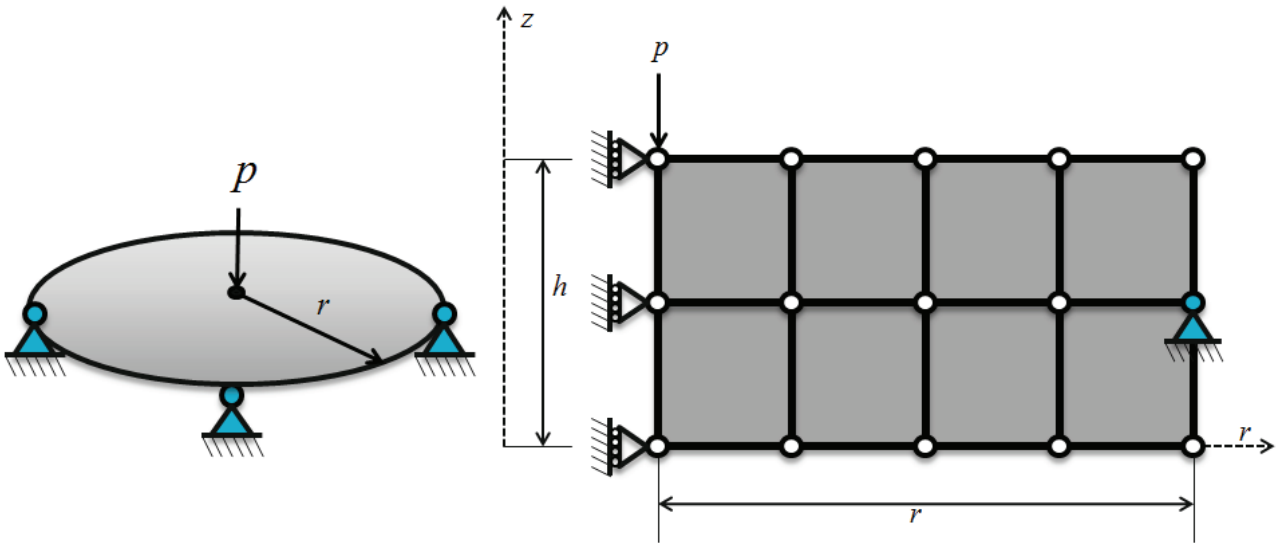

Figure 8. Simply supported circular plate with point load

$$
\begin{aligned}
u_z &= \frac{P}{16\pi D}\left[\frac{3+\nu}{1+\nu}\left(R^2-r^2\right)+2r^2 log\left(\frac{r}{R}\right)\right] \\
u_r &= 0 \\
D &= \frac{Eh^3}{12\left(1-\nu^2\right)} \\
\sigma_r &= \frac{12M_r z}{h^3} \\
\sigma_\theta &= \frac{12M_\theta z}{h^3} \\
M_r &= \frac{P}{4\pi}(1+\nu)\log\left(\frac{R}{r}\right) \\
M_\theta &= \frac{P}{4\pi}\left[(1+\nu)\log\left(\frac{R}{r}\right)+1-\nu\right]
\end{aligned}
\tag{38}
$$

Likewise, u_z represents for the axial displacement, D is the stiffness modulus of the plate, σ_r is the radial stress, σ_θ is the hoop stress, M_r is represented for the couple in the radial direction and M_θ is the couple in the circumferential direction. Fig. 9 illustrates the profile of displacement along the radius of the plate. The obtained numerical results show the slight difference with the analytical results. Since the hybrid finite element method is considerably affected by the selection of stress function, the obtained numerical results may have lost their accuracies based on the employed stress approximation function. Based on this results it can be concluded that in hybrid formulation the stress function is specific for each

problem and it should be estimated separately for each specific problem. Fig .10 represents the contour plot of radial stress through the radius of the circular plate. Fig. 11 shows the accuracy of the obtained numerical results in comparison with the analytical solution.

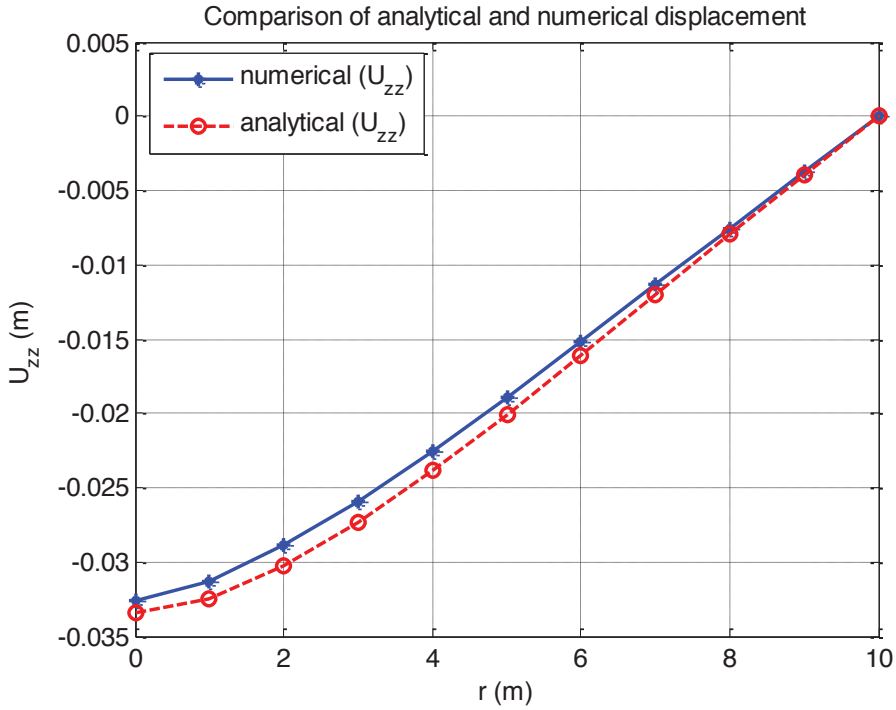

Figure 9. Comparison of analytical and numerical displacement – U_{zz}

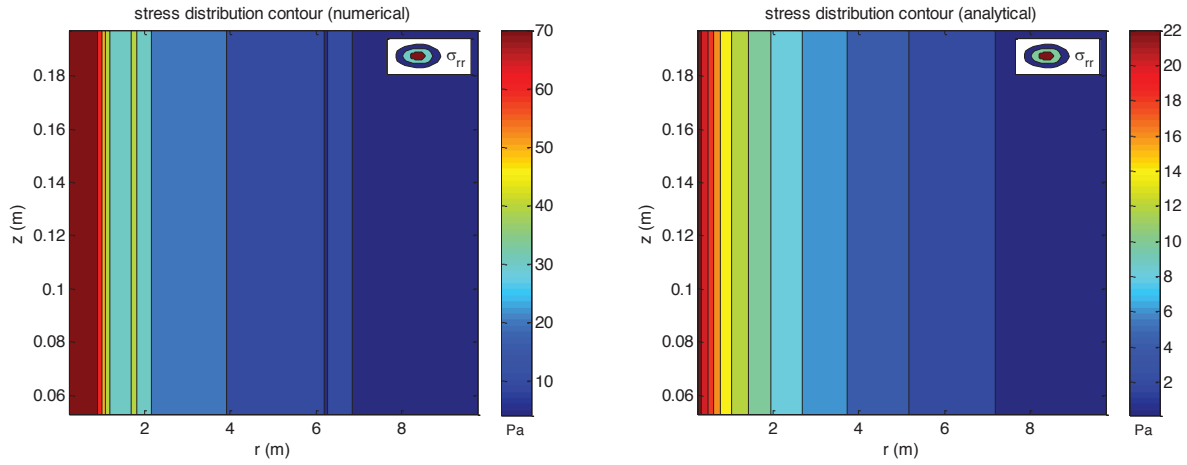

Figure 10. Radial stress distribution contour (σ_{rr}) – numerical & analytical results

It can be observed that the obtained radial stress just following the trend of analytical stress. Moreover, under the point load the prediction finite element analysis is not acceptable at all due to the applied concentrated force there.

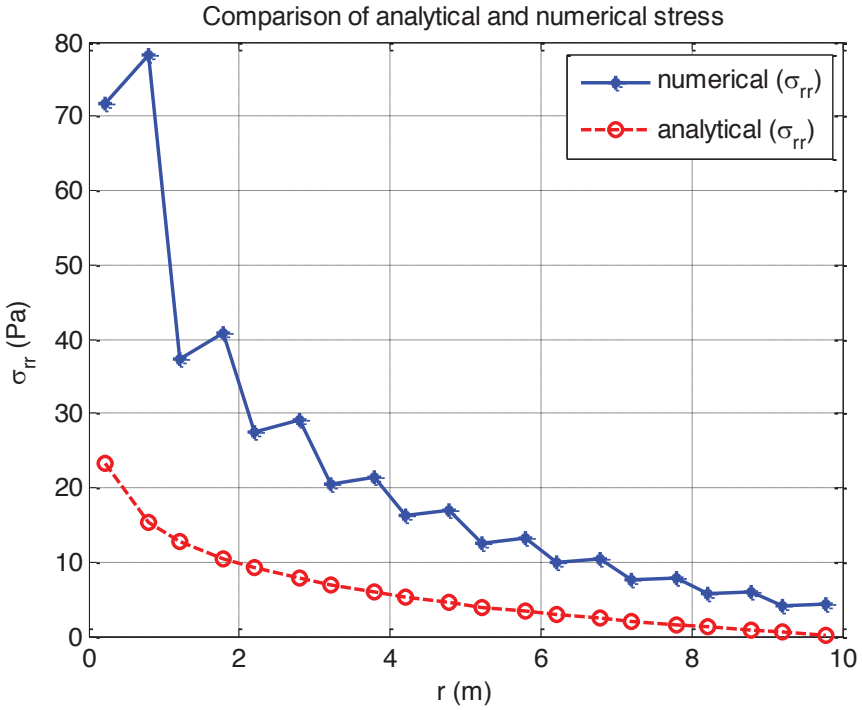

Figure 11. Comparison of analytical and numerical stress (σ_{rr})

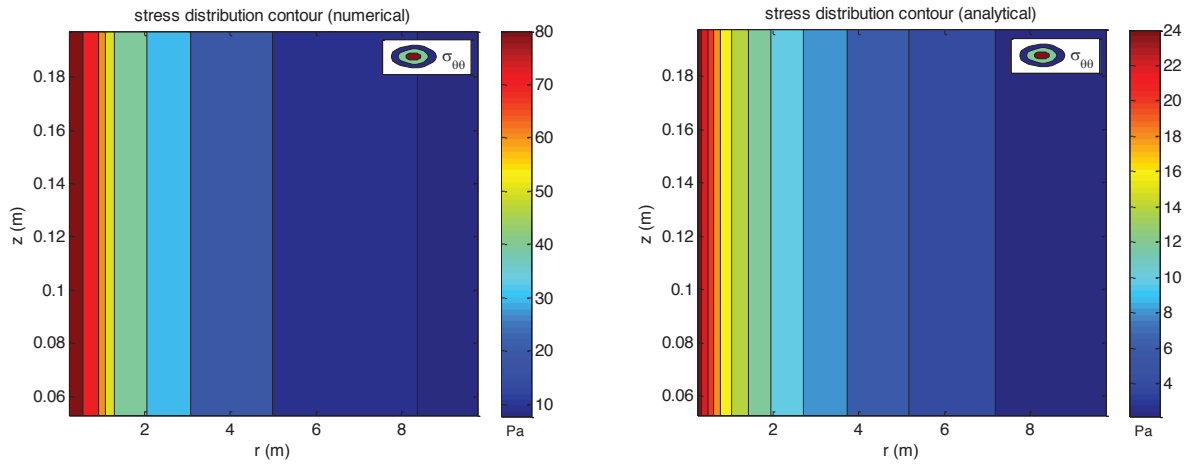

Figure 12. Circumferential stress distribution contour ($\sigma_{\theta\theta}$) – numerical & analytical results

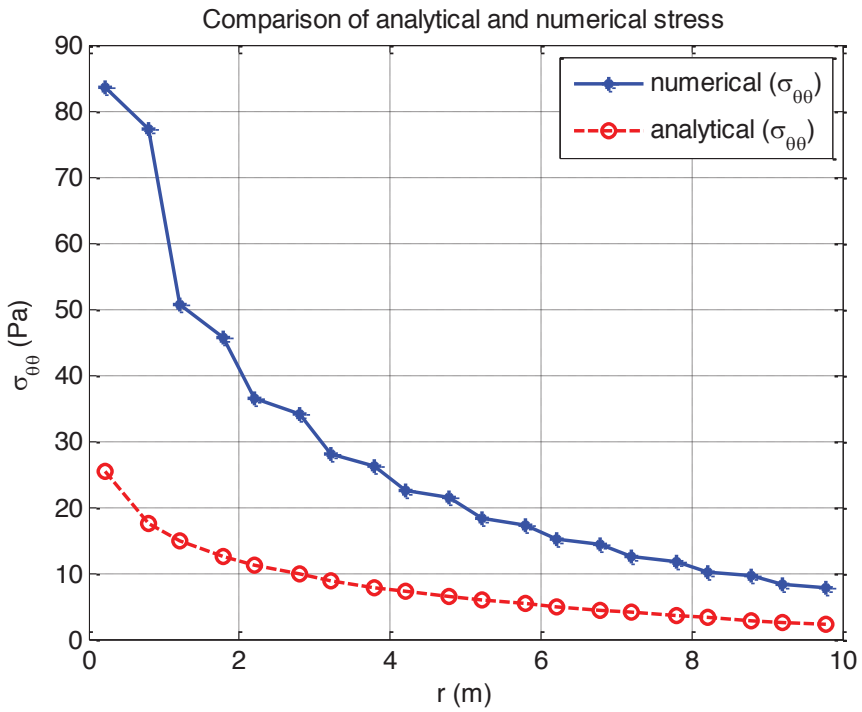

Figure 13. Comparison of analytical and numerical stress ($\sigma_{\theta\theta}$)

Fig. 13 illustrates the profile of hoop stress along the radius of the circular plate. Similar to the radial stress the predicted stress is in good agreement with the analytical results in the region far from the point load. Thus, from this analysis it can be found out that the employed stress function is not capable of capturing the stress around the point load as it overestimates the stress around the point load.

Benchmark No.3: Clamped circular plate with point load

In this section, the cantilever circular plate under point load is simulated by the hybrid finite element method. The developed element with the similar stress function is used to capture the stress and displacement fields. Fig. 14 illustrates the geometrical configuration and the schematic of the employed mesh. It is to be noted that for the clamped boundary condition the displacement degrees of freedom in the radial and the axial direction are fixed.

Table 3. The geometrical and material properties for the simply supported circular plate

Input Parameters	***r (m)***	***h (m)***	***E (N/m^2)***	***v***	***p***
Values	4.0	0.5	1.0e+05	0.4999999	10

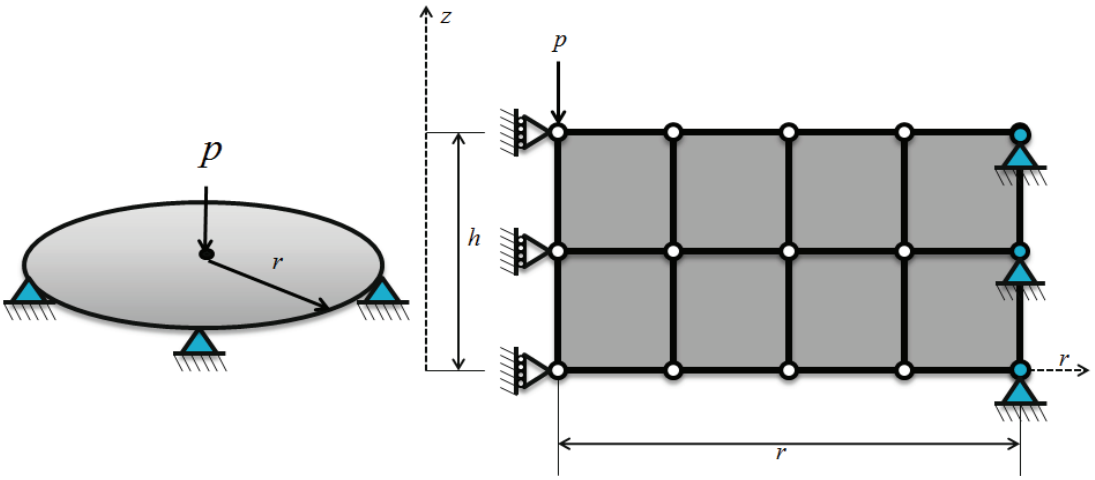

Figure 14. Clamped circular plate with point load

The analytical solution can be found in Timoshenk [4], the expressions for displacement and stress can be written as follows

$$
\begin{aligned}
u_z &= \frac{P}{8\pi D} r^2 log\left(\frac{r}{R}\right) + \frac{P}{16\pi D}\left(R^2 - r^2\right) \\
u_r &= 0 \\
D &= \frac{Eh^3}{12\left(1-\nu^2\right)} \\
\sigma_r &= \frac{12 M_r z}{h^3} \\
\sigma_\theta &= \frac{12 M_\theta z}{h^3} \\
M_r &= \frac{P}{4\pi}\left[\left(1+\nu\right)\log\left(\frac{R}{r}\right) - 1\right] \\
M_\theta &= \frac{P}{4\pi}\left[\left(1+\nu\right)\log\left(\frac{R}{r}\right) - \nu\right]
\end{aligned}
\tag{39}
$$

In which u_z represents for the axial displacement, D is the stiffness modulus of the plate, σ_r is the radial stress, σ_θ is the hoop stress, M_r is represented for the couple in the radial direction and M_θ is the couple in the circumferential direction. Fig. 15 illustrates the radial

displacement field through the radius of the circular plate. It can be observed that the difference between the hybrid finite element results and the analytical solution is considerable. The obtained results for the displacement proves the fact that the employed 4-node quadrilateral element for the prediction of displacement in this problem is not enough and we need to employ the higher order element. Fig. 16 and 19 illustrates the profile of stress with respect to the radius of the circular plate. Similar to the previous case the stress of the finite element analysis in the vicinity of the point load is not in agreement with analytical data, However in the region far from the point load the prediction of stress in close to the analytical data.

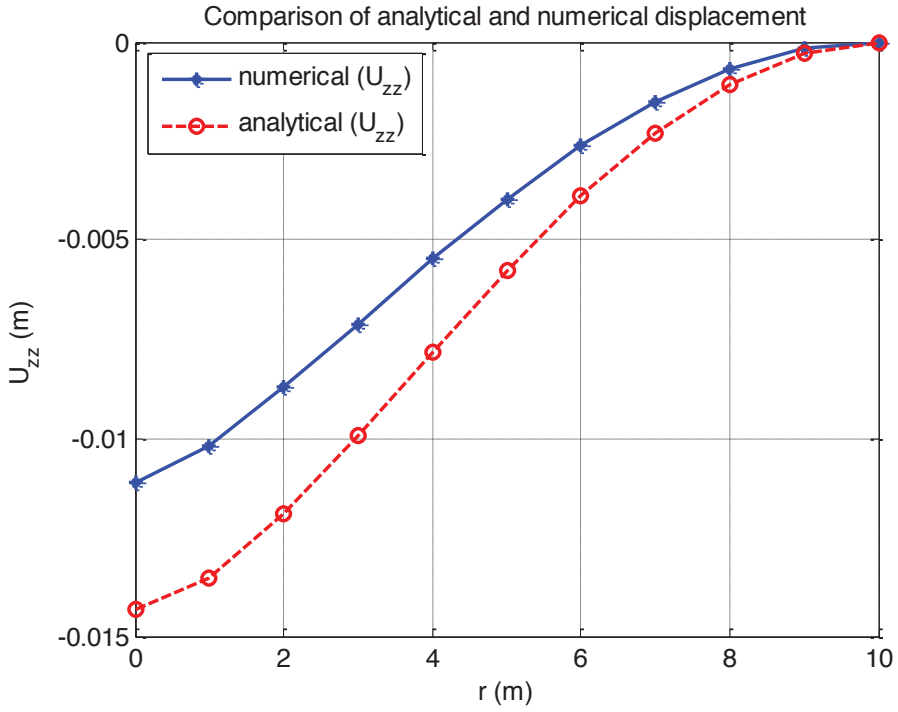

Figure 15. Comparison of analytical and numerical displacement – U_{zz}

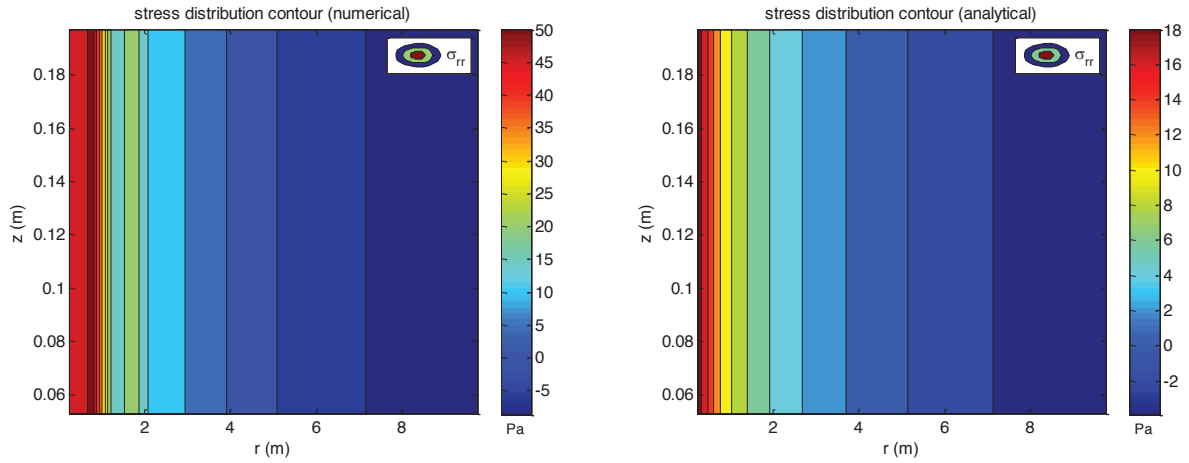

Figure 16. Radial stress distribution contour (σ_{rr}) – numerical & analytical results

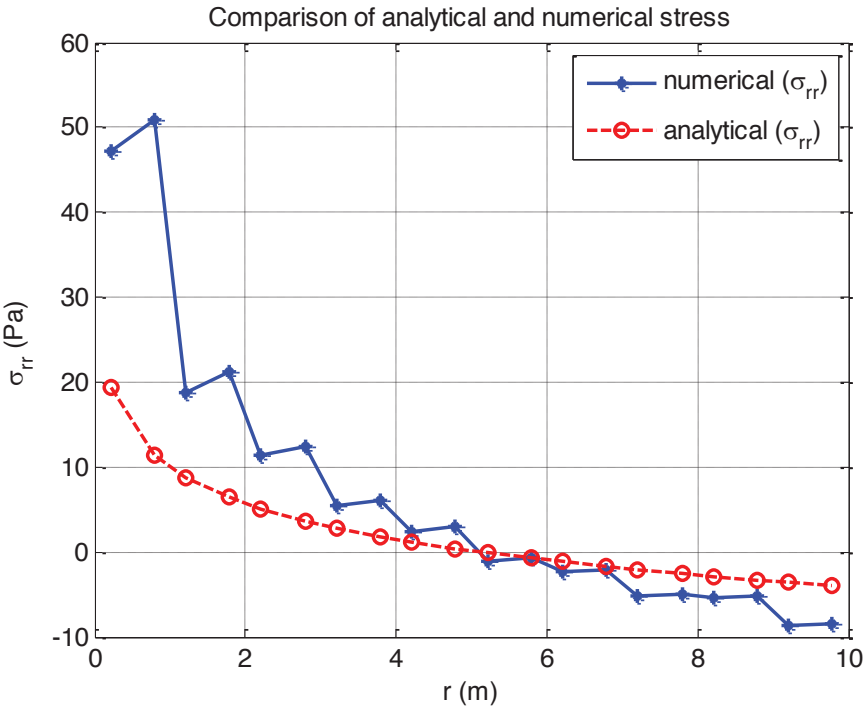

Figure 17. Comparison of analytical and numerical stress (σ_{rr})

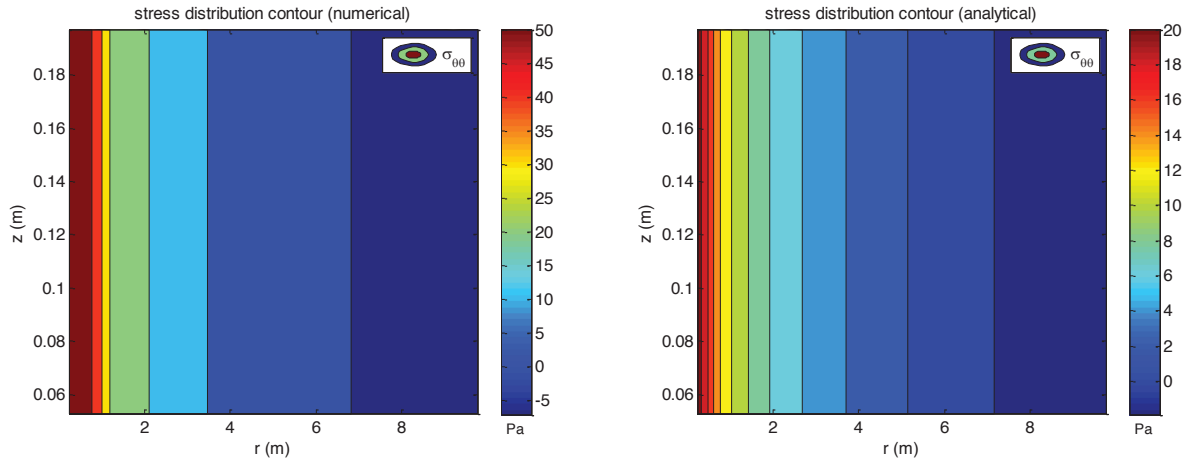

Figure 18. Circumferential stress distribution contour ($\sigma_{\theta\theta}$) – numerical & analytical results

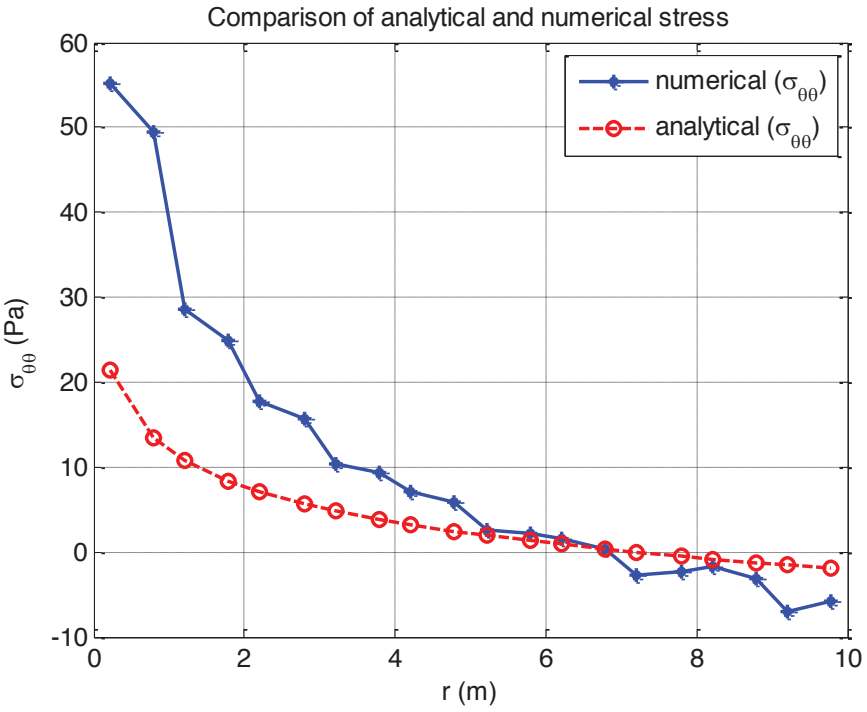

Figure 19. Comparison of analytical and numerical stress ($\sigma_{\theta\theta}$)

Based on the obtained numerical results in this analysis it can be found out that the usage of the stress function is dependent on the boundary condition and the applied load. Since in the two considered circular plate the accuracies obtained by the same stress function were different.

Conclusion

In this project, the 4-node quadrilateral axisymmetric element is developed based on the hybrid element formulation. The developed element has the two master field of displacement and stress. Thus, we need to come up with two approximation functions for the displacement and stress. The performance of this formulation is mainly affected by the stress approximation function. The obtained numerical results for the under pressure thick wall cylinder were in excellent agreement with analytical results. However, in the other two circular plates the obtained numerical were not as good as they should be.

References

[1] Felippa, C. A., "Advanced Finite Element Methods (lecture notes)." University of Colorado at Boulder Department of Aerospace Engineering, 2013.

[2] Renganathan K., Nageswara Rao B., Jana M.K. "An efficient axisymmetric hybrid-stress displacement formulation for compressible / nearly incompressible material." International Journal of Pressure Vessels and Piping 77 (2000) 651–667.

[3] Jog C. S., Annabattula R. " The development of hybrid axisymmetric elements based on the Hellinger–Reissner variational principle." Int. J. Numer. Meth. Engng 65 (2006) 2279 2291.

[4] Timoshenko, S., and S. Woinowsky-Krieger. "Theory of Plates and Shells." McGrawHill Book Company, Inc., 1959.